Confining light with negative refraction in checkerboard metamaterials and photonic crystals

S. Anantha Ramakrishna,[1,2] S. Guenneau,[2,3] S. Enoch,[2] G. Tayeb,[2] and B. Gralak[2]
[1]*Department of Physics, Indian Institute of Technology, Kanpur 208016, India*
[2]*Institut Fresnel, UMR CNRS 6133, Universités Aix-Marseille I & III, 13397 Marseille Cedex 20, France*
[3]*Department of Mathematical Sciences, Liverpool University, Liverpool L69 3BX, United Kingdom*
(Received 19 September 2006; published 28 June 2007)

We present here a finite slab of triangular checkerboard of negative refractive index material that exhibits a form of extraordinary transmission. We show that such a checkerboard can be used to confine light and can act as an open resonator. Effectively even a single point of intersection between three triangular wedges of negative refractive index may act as a resonator that confines light in the limit when n tends toward -1. We find that the quality of the confinement improves by adding more triangular wedges around the initial point in a checkerboard fashion. The confinement effect is also demonstrated by using a photonic crystal that shows the negative refraction effect.

DOI: 10.1103/PhysRevA.75.063830 PACS number(s): 42.70.Qs, 78.20.Ci

In 1967, Veselago wrote a visionary paper in which materials with simultaneously negative permittivity (ε) and magnetic permeability (μ) were shown to have a negative refractive index [1]. It was shown by a ray analysis that a slab of a negative refractive index material (NRM) can act as a flat lens that imaged a source on one side to a point on the other. But this result remained an academic curiosity for almost thirty years, until Pendry and co-workers [2,3] proposed designs of structured materials which would have negative ε and μ. The experimental demonstration of such materials subsequently at GHz frequencies [4,5] provided a fillip to research in this area (see [6] for a recent review). These so-called metamaterials are structured at subwavelength lengthscales (typically $\lambda/10$), hence it is possible to regard them as almost homogeneous. Using photonic crystals (PC) [7], a very similar negative refraction effect at all angles of incidence was independently predicted in [8–11].

In a seminal paper, Pendry demonstrated that the Veselago slab lens not only involves the propagative waves but also the evanescent near-field components of a source in the image formation [12]. Such a superlensing effect has been demonstrated at optical frequencies through a silver slab film in [13] (resolution of $\lambda/5$). It was then shown by Pendry and Ramakrishna [14] that the superlensing effect with a slab of negative refractive index medium can be generalized to materials which are spatially inhomogeneous. The only condition is that the system has to respect a mirror antisymmetry about a plane normal to the imaging axis. Using a geometric technique it was shown [14], as a consequence of this theorem, that two rectangular (semi-infinite) intersecting wedges of NRM acts as an imaging system whereby a source gets imaged onto itself. This system, originally studied by Notomi [10] using a ray picture, was thus shown to involve the evanescent modes also and act as a unique resonator. Guenneau *et al.* [15] subsequently generalized this imaging effect to a rectangular checkerboard lattice where alternating cells have positive ($\varepsilon=\mu=+1$) and negative ($\varepsilon=\mu=-1$) refractive index. It was shown that a source placed in one cell would reproduce itself in every other cell of the infinite lattice. The properties of corners and checkerboards in the presence of dissipation have also been studied [16,17]. Monzon *et al.* [18] recently derived an analytical solution for a finite sized NRM wedge in the presence of a source. He *et al.* [19] studied some modes of a resonator with NRM wedges and constructed an open cavity using triangular wedges of a PC that shows the negative refraction effect.

In this paper, we show that light can be confined in a finite checkerboard of NRM. A single intersecting corner of finite wedges can support leaky modes, and this leakage can be reduced by putting an additional layer of wedges around the central intersection point. Thus light can be strongly confined in the interior of such systems. Due to geometry, a triangular checkerboard presents some advantage over a rectangular checkerboard in this regard. We demonstrate this effect using

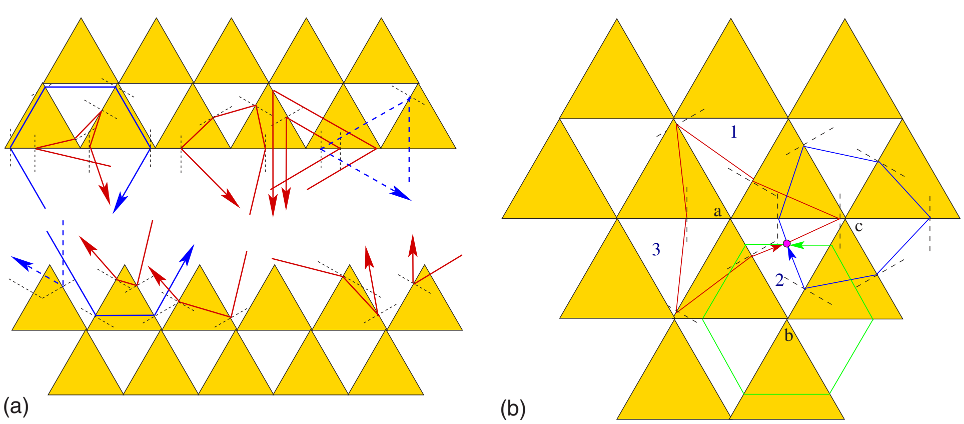

FIG. 1. (Color online) Left panel: All rays incident on the checkerboard from below (upper left) and from above (lower left) are reflected. Right panel: All rays emitted by a source in the checkerboard are trapped (closed trajectories around corners).

TABLE I. Samples of resonant wavelengths λ computed with FEM for nondissipative finite checkerboards consisting of square (■) and triangular (△) cells of side $a=0.1$, i.e., the wavelengths λ considered are fifty times larger than a. The number of cells of the checkerboards with negative refractive index ($n=-1$) material (same number as cells with refractive index $n=1$) appears in the first column. Also, (*) and (**) denote respectively upper left and right modes of Fig. 2.

NRM checkerboard	Square (■)	Triangular (△)
2■/3△(*)	$4.732+i0.816$	$4.844+i0.795$
2■/3△(**)	$4.645+i0.822$	$4.794+i0.802$
8■/12△	$5.046+i0.218$	$4.999+i0.036$
18■/27△	$4.951+i0.044$	$4.973+i0.006$

triangular wedges of PC which display the negative refraction effect.

As a preamble, let us consider a finite checkerboard of NRM ($n=-1$) with rectangular cells. It is clear from a ray picture that a large subset of the rays emanating from a source placed in one of the cells will always emerge out of the structure [15]. Although there are other ways of tiling the plane, the crystallographic restriction and the balance between overall positive and negative regions imply that we are left with only rectangular, square or (equilateral) triangular cells. For a finite checkerboard of triangular cells, the ray pictures predict that the rays from a source placed in one of the interior cells cannot escape from the structure if the intersection of the wedges is completely surrounded by other points of intersection (see Fig. 1, right panel). This suggests that such a system will very strongly confine light. However, a word of caution about the ray picture in such singular systems would be in order. Consider two optically complementary layers [14] made of triangular wedges as shown in Fig. 1, left panel. The ray picture clearly shows that all incident rays should be reflected from the structure while the full wave calculation of the complementary theorem [14,15] predicts that the structure should have unit transmission for all waves and will have zero reflectivity (see also [20] for a similar paradigm). In fact, such a structure is an example of a checkerboard lens which will exhibit subwavelength imaging and extraordinary transmission through excitations of plasmon resonances (see [16] for transmission properties of dissipative square checkerboards). Nevertheless, the type of plasmonic guidance involved here via the interfaces between positive and negative index media differs substantially from the extraordinary transmission through subwavelength holes in thick metallic films experimentally demonstrated in [21], as we shall see in the sequel. As illustrated by the paradox of the ray picture showing no transmission and the complementary theorem showing perfect lensing (the optical path cancels), it is imperative to investigate numerically finite structures of NRM which are of the checkerboard type.

First, we look at the eigenfunctions associated with a finite checkerboard structure consisting of square and triangular cells of homogeneous NRM media. We model the spectral problem using the finite element package FEMLAB which solves Maxwell's system in unbounded domain with

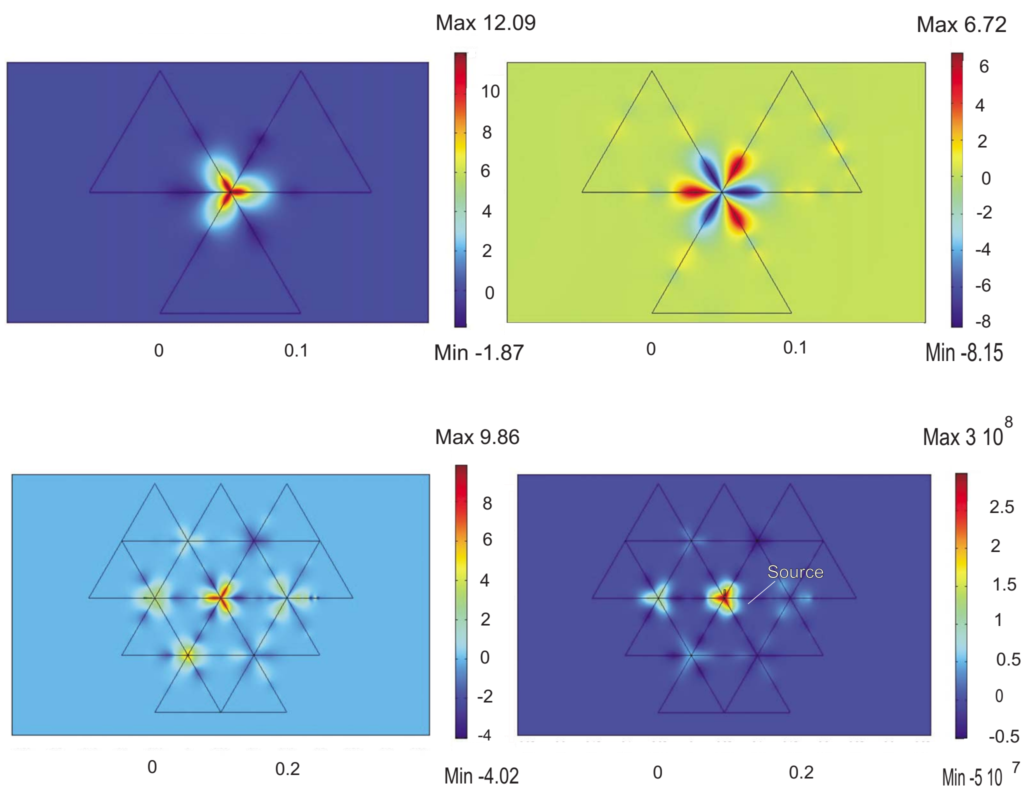

FIG. 2. (Color online) Resonant modes of triangular checkerboards with cells of sidelength $a=0.1$. Upper left: $\lambda=4.844+i0.795$. Upper right: $\lambda=4.794+i0.802$. Bottom left: $\lambda=4.999+i0.036$. Bottom right: Harmonic line source at wavelength $\lambda=4.999$ (see Table I).

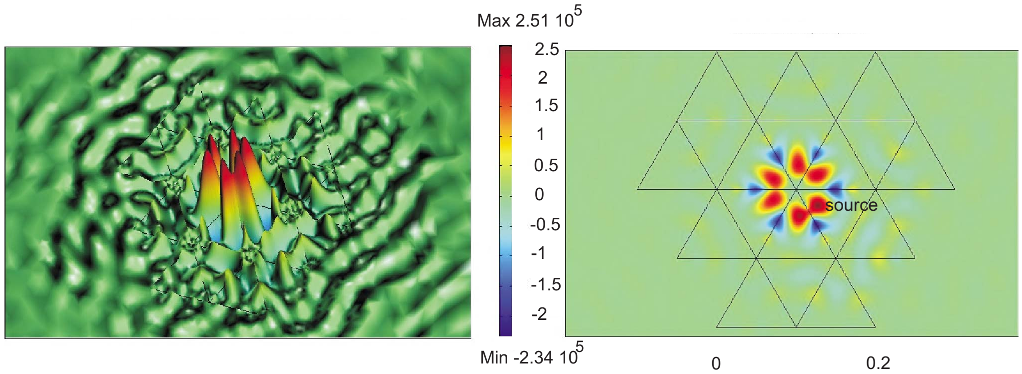

FIG. 3. (Color online) Field radiated by a line source of wavelength $\lambda = 0.05 = a/2$ within a checkerboard with dissipative NRM ($\varepsilon = \mu = -1 + i4 \times 10^{-6}$).

perfectly matched layers [22]. Eigenfrequencies are in general complex with an imaginary part accounting for the leakage in a nondissipative medium. In Table I, we list the real and imaginary parts of wavelengths of a small number of sample modes obtained for the systems shown in Fig. 2 (there is an infinite number of such leaky modes as the spectrum associated with this problem is continuous). We observed in these calculations that the eigenfunctions are large in magnitude at the intersecting corners and very small in the bulk of the material. The working wavelength is typically fifty times larger than the cell's size, so that these corner modes are exponentially decaying away from the corners. We observe some surface plasmon excitations running along the interfaces separating complementary media. Since there is a large degeneracy of the modes, the leaky modes could be localized at any corner. From Table I, we see that the ratio of the real part to the imaginary part of some *representative* eigenfrequencies increases with increasing size of the checkerboard (i.e., the leakage reduces). The rate of increase is faster for the case of triangular structure. From Fig. 2, we see that the amplitude of the cornermode increases with the size of the system (actually it goes up faster for triangular than for square lattices).

Second, we investigate the electromagnetic response of such finite checkerboards to a line source located inside one of their cells (with positive refractive index). We numerically checked that line sources excite the complex eigenmodes of the nondissipative checkerboards as seen in Fig. 2, bottom right corner. Indeed, when the (real) frequency of a harmonic line source is sufficiently close to the real part of the leaky mode of the finite checkerboard, they do couple together. In this case, plasmons convey subwavelength details of the source which is reproduced in every other cell of the checkerboard. Nevertheless, the singular behavior of the field at every corner somehow masks the imaging process. Hence we introduce some small dissipation in every cell with negative ϵ and μ to help figuring out how plasmon resonances build up the images. For smaller wavelengths (typically one-half of the cell's size), we can see from Fig. 3 that images of the line source located in a cell of the checkerboard start forming in every other cells, as it was predicted from the ray analysis in Fig. 1: For larger wavelengths, evanescent components of the source become primarily important to build up images, which start appearing only in large checkerboards (a complex network of plasmon resonances needs to take place). The 2D plot of Fig. 3 compares very well with results reported in [17] for a perfect corner reflector.

Finally, we explore light confinement through negative refraction in such finite checkerboards when we replace the NRM by a photonic crystal that displays the all angle nega-

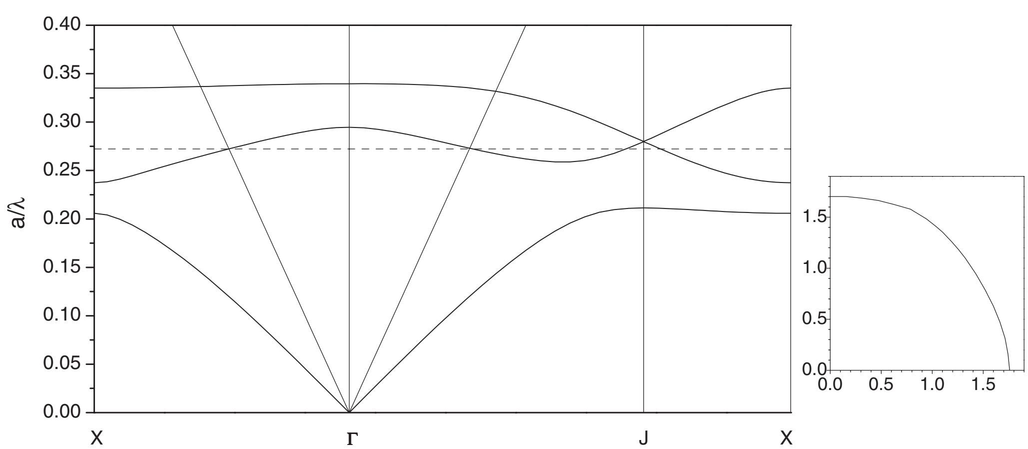

FIG. 4. Dispersion diagram for a triangular array of circular rods $r = 0.45a$, where a the period. Horizontal axis: Bloch vector describing the first Brillouin zone ΓJX. Vertical axis: Normalized frequencies a/λ, with λ the wavelength. Inset: Iso frequency contour at intersection of light line with optical band showing negative group velocity at $\lambda = 3.66a$.

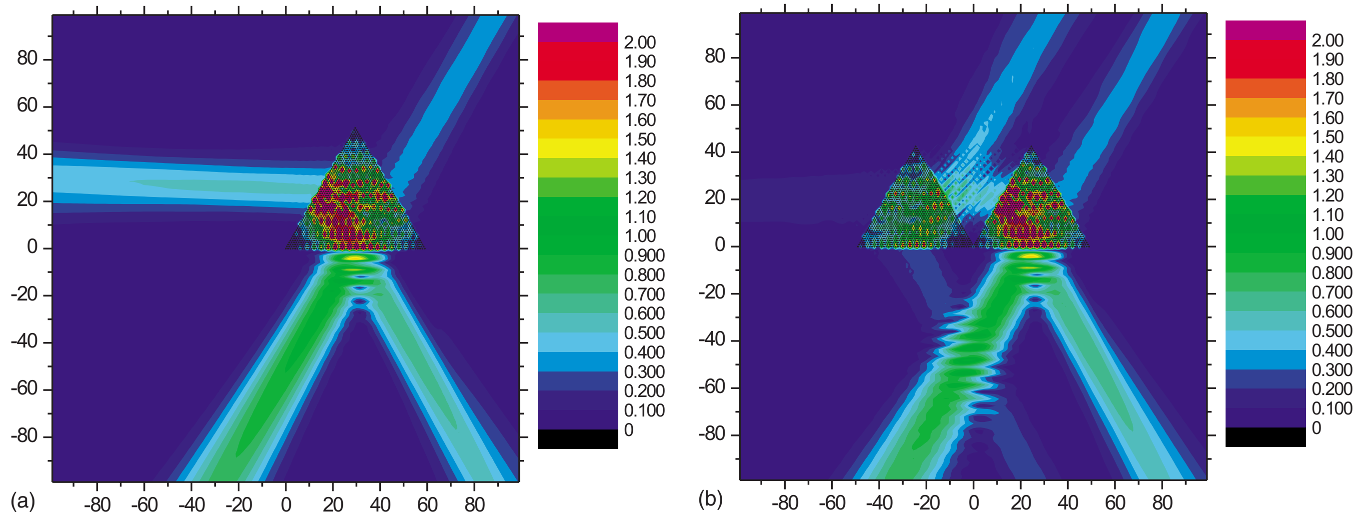

FIG. 5. (Color online) Left: Gaussian beam of wavelength $\lambda = 3.6798a$ incident from the left on a PC triangle of pitch array a, making an angle of 30° with the vertical axis. It is centered on the middle of the triangle side (consisting of 60 rods) and its width is $20a$. Right: Same with two triangles with 50 rods on their sides.

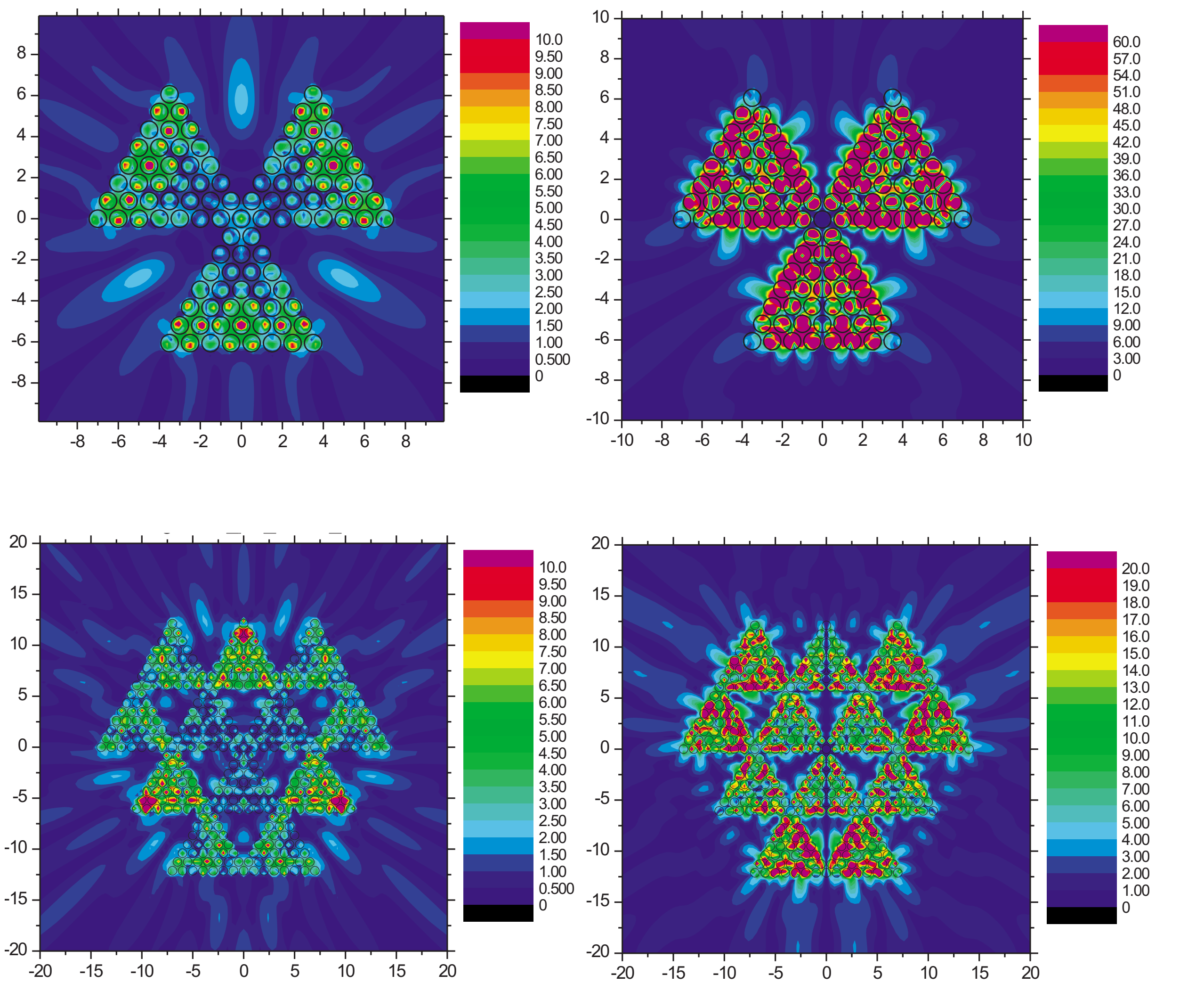

FIG. 6. (Color online) Upper panel: Resonance modes for 3 PC triangles of pitch array a at wavelengths $\lambda = 3.67976a + i0.21139a$ (left) and $\lambda = 3.74735a + i0.000603a$ (right). Lower panel: Resonance modes for 12 triangles at wavelengths $\lambda = 3.68176a + i0.007727a$ (left) and $\lambda = 3.67965a + i0.002369a$ (right).

tive refraction effect. We consider a triangular array of cylindrical fibers of circular cross-section and high-refractive index ($n=4$) embedded within an air matrix. We meet the criteria for all-angle negative refraction in p polarization (the magnetic field is parallel to the axis of cylinders) for a pitch array a and fibres' radii $r=0.45a$ at $\lambda=3.66a$ (see Fig. 4). The essential condition for the all angle negative refraction (AANR) effect is that the equifrequency surfaces (EFS) should become convex everywhere about some point in the reciprocal space, and the size of this EFS should shrink with increasing frequency. Further the frequency should be within the first Bragg zone. The negative refraction effect can be clearly seen on Fig. 5, left panel, where a gaussian beam of light of wavelength $\lambda=3.6798a$ is incident on a triangle from the left, making an angle of 30° with the vertical axis. It is centered on the middle of the triangle side (consisting of 60 rods) and its width is $20a$. On the right panel of Fig. 5 the same beam is transmitted backwards to the right with a 30 degrees angle with the vertical axis. The multiple beams arise due to finite reflection at the air-PC interfaces. The negatively refracted beam in the right panel is actually the weakest one to emerge. Using such composite triangles as building blocks of checkerboards, we now look for confined modes due to all angle negative refraction. For this, we look for resonance poles in the complex frequency planes in the vicinity of the negative refraction band of Fig. 4: For the corresponding finite PC checkerboard, the phenomenon attenuates due to leakage (complex poles). The resonance poles were found thanks to an algorithm discussed in [23] (note that AANR occurs only around a given frequency for infinite PC). For a line source operating on resonance close to the intersection of surface band with light cone, surface states at interfaces between PC and air dominate: a large field amplitude can be seen on Fig. 6. The finite reflectivity observed at the PC terminations is due to impedance mismatch between PC and air. This effect may be reduced by changing the rod's shapes on the interfaces between PC and air (as proposed in [19]) or otherwise by increasing the size of the structure. Importantly, the amplitude of the field in the middle corner becomes really large when the line source excites checkerboard resonances. On the other hand, when the field radiated by the line source no longer couples with the checkerboard resonances, it starts filling up the overall PC region through total internal reflection (effective index larger than that of air). In this case the field vanishes in the middle corner, as seen on Fig. 6 and the leakage is reduced. To

TABLE II. Samples of normalized energy W/W_0, power radiated P/P_0, and confinement time T/T_0 computed for a line source radiating at wavelengths $3.67983a$ (3△) and $3.67964a$ (12△) over a square area of sidelength $32a$ included in a PC checkerboard of pitch array a corresponding to upper left and lower right diagrams of Fig. 6. (*) and (**) denote respectively line sources located at (0,5.78) and (0,4).

PC checkerboard	Energy W/W_0	Power P/P_0	Time T/T_0
3△(*)	5.4901	1.1756	4.6702
3△(**)	5.5356	0.7810	7.0879
12△(*)	93.840	4.1484	22.621
12△(**)	8.6088	0.4310	19.974

demonstrate the improvement of light confinement through enlargement of PC checkerboards, we finally compute their cavity lifetime by evaluating first the total electromagnetic energy W over a given *fixed domain* Ω (here a square of side length $32a$) including the checkerboard and a wire source and normalizing it with that of the source in vacuum W_0 (see Table II). We then compute the power P radiating away from the structure by integrating the Poynting vector flux over $\partial\Omega$ and normalizing it by the power P_0 when the checkerboard is removed (source in vacuum). The normalized cavity lifetime is then given by $T/T_0=WP_0/(W_0P)$. Numerical results showing improvement of cavity lifetime when we increase the size of the checkerboard are reported in Table II. We also note its dependence upon the position of line source.

To conclude this paper, we would like to emphasize that the checkerboard structures we introduce offer a unique way to confine light through negative refraction, as was checked both for finite checkerboards of nondissipative homogeneous NRM with the finite element method, and for composite checkerboards exhibiting AANR with the scattering matrix approach. As a corollary of the decrease of the imaginary part of λ when we add up cells around a line source in the checkerboard (see Table I, Table II, and Fig. 6), the cavity lifetime will improve.

S.A.R. acknowledges partial support from the Department of Science and Technology, India under Grant No. SR/S2/CMP-54/2003. S.G., S.E., G.T., and B.G. acknowledge funding from the EC funded project PHOREMOST under grant FP6/2003/IST/2-511616.

[1] V. G. Veselago, Usp. Fiz. Nauk **92**, 517 (1967).
[2] J. B. Pendry, A. J. Holden, D. J. Robbins, and W. J. Stewart, Phys. Rev. Lett. **76**, 4773 (1996).
[3] J. B. Pendry, A. J. Holden, W. J. Stewart, and I. Youngs, IEEE Trans. Microwave Theory Tech. **47**, 2075 (1999).
[4] D. R. Smith, W. J. Padilla, D. C. Vier, S. C. Nemat-Nasser, and S. Schultz, Phys. Rev. Lett. **84**, 4184 (2000).
[5] C. G. Parazzoli, R. B. Greegor, K. Li, B. E. C. Koltenbah, and M. Tanielian, Phys. Rev. Lett. **90**, 107401 (2003).
[6] S. A. Ramakrishna, Rep. Prog. Phys. **68**, 449 (2005).
[7] E. Yablonovitch, Phys. Rev. Lett. **58**, 2059 (1987).
[8] R. Zengerle, J. Mod. Opt. **34**, 1589 (1987).
[9] B. Gralak, S. Enoch, and G. Tayeb, J. Opt. Soc. Am. A **17**, 1012 (2000).
[10] M. Notomi, Opt. Quantum Electron. **34**, 133 (2002).
[11] C. Luo, S. G. Johnson, J. D. Joannopoulos, and J. B. Pendry, Phys. Rev. B **65**, 201104(R) (2002).
[12] J. B. Pendry, Phys. Rev. Lett. **85**, 3966 (2000).

[13] N. Fang, H. Lee, C. Sun, and X. Zhang, Science **308**, 534 (2005).
[14] J. B. Pendry and S. A. Ramakrishna, J. Phys.: Condens. Matter **15**, 6345 (2003).
[15] S. Guenneau, A. C. Vutha, and S. A. Ramakrishna, New J. Phys. **7**, 164 (2005).
[16] S. Chakrabarti, S. A. Ramakrishna, and S. Guenneau, Opt. Express **14**, 12950 (2006).
[17] S. Guenneau, B. Gralak, and J. B. Pendry, Opt. Lett. **30**, 1204 (2005).
[18] C. Monzon, D. W. Forester, and P. Loschialpo, Phys. Rev. E **72**, 056606 (2005).
[19] S. He, Y. Jin, Z. Ruan, and J. Kuang, New J. Phys. **7**, 210 (2005).
[20] J. B. Pendry, Contemp. Phys. **45**, 191 (2004).
[21] L. Martin-Moreno, F. J. Garcia-Vidal, H. J. Lezec, K. M. Pellerin, T. Thio, J. B. Pendry, and T. W. Ebbesen, Phys. Rev. Lett. **86**, 1114 (2001).
[22] J. P. Berenger, J. Comput. Phys. **114**, 185 (1994).
[23] G. Tayeb and D. Maystre, J. Opt. Soc. Am. A **14**, 3323 (1997).